Received April 19, 2019, accepted May 19, 2019, date of publication May 29, 2019, date of current version July 1, 2019.

Digital Object Identifier 10.1109/ACCESS.2019.2919750

Simulation Research on Exploiting Electrostatic Potential Difference Sensing for Shaft Centerline Orbit Reconstruction

KAIHAO TANG[1], HONGLI HU[1], (Member, IEEE), LIN LI[1], YONG QIN[2], AND XIAOXIN WANG[3]

[1]State Key Laboratory of Electrical Insulation and Power Equipment, Xi'an Jiaotong University, Xi'an 710049, China
[2]State Key Laboratory of Rail Traffic Control and Safety, Beijing Jiaotong University, Beijing 100044, China
[3]Key Laboratory of Education Ministry for Photoelectric Logging and Detecting of Oil and Gas, Xi'an Shiyou University, Xi'an 710065, China

Corresponding author: Hongli Hu (hlhu@mail.xjtu.edu.cn)

This work was supported in part by the National Natural Science Foundation of China under Grant 51777151, in part by the National Key R&D Program of China under Grant 2016YFB0901200, in part by the Open Research Fund of State Key Laboratory of Rail Traffic Control and Safety under Grant RCS2017K006, in part by the Shaanxi Provincial Key Technologies R&D Programme under Grant 2016GY-001, in part by the Scientific Research Program Funded by Shaanxi Provincial Education Department under Grant 18JK0606, and in part by the Fundamental Research Funds for the Central Universities under Grant xzy022019046.

ABSTRACT To realize the non-contact measurement of the rotational shaft centerline orbit, a shaft centerline orbit reconstruction method using a specifically designed electrostatic sensor in conjunction with the neural network approximator is proposed in this paper. The sensing principle of the designed electrostatic sensor is based on the partial capacitance theory. The proposed sensor consists of one electrostatic field excitation electrode, two sensing electrodes, and a cylindrical metal shield covering the three electrodes. It directly establishes the map from the sensor output (voltages between sensing electrodes and shield) to shaft center position through the neural network approximator so that the shaft centerline orbit can be reconstructed. The CAE software COMSOL Multiphysics is used for sensor modeling and simulation analysis. The simulation reconstruction experiment is carried out to test the performance of the proposed sensor and to obtain training data for the neural network. The experiment result shows that the RMS error of the proposed sensor is within 0.4 μm, which has proved the feasibility of the novel sensor combined with the neural network fitting algorithm for industrial applications.

INDEX TERMS Electrostatic sensor, neural network, rotational machinery, shaft centerline orbit.

I. INTRODUCTION

Rotor-bearing system is key component of rotational machineries which are widely used in various industrial process. Therefore, rotor-bearing condition monitoring and fault diagnosis technology is significant to almost all industrial areas. Shaft centerline orbit is usually adopted as a kind of important data to analyze the state of a rotor-bearing system because it involves abundant shaft condition information. Generally, rotor faults include misalignment, unbalance, and rub-impact, all of which can be figured out by properly analyzing shaft centerline orbit [1], [2].

The most widely used method of shaft centerline measurement is to synthesize the axial trajectory using two mutually orthogonal vibration displacement signals in the same cross section of the shaft. To get the two vibration displacement signals, a common method is to directly measure vibration displacement signal through eddy current displacement sensors [3], [4]. Using eddy current sensors to realize shaft centerline orbit monitoring has high precision, but the equipment is expensive and sensor setup is complex.

Electrostatic sensor is a kind of widely used low-cost and non-contacting sensor [5], [6]. Recently, some researcher begin to study how to use electrostatic sensor for rotational machinery condition monitoring. Wang *et al.* [7] put forward a novel application of electrostatic sensors of rotational speed measurement conjunct with signals cross-correlation algorithm. The main principle of this method is to estimate the time-lag between the two sensors arranged angled surrounding the shaft by α in radians conjunct with cross-correlation algorithm. Based on signals cross-correlation algorithm, Li *et al.* [8] developed double correlation technique for

The associate editor coordinating the review of this manuscript and approving it for publication was Gongbo Zhou.

rotational speed measurement, with improvement in accuracy and robustness. Later, Hu *et al.* [9] proposed an application of strip-shape-electrode electrostatic sensors array for belt vibration measurement.

Inspired by electrostatic sensor's being used for rotational speed and vibration monitoring, a specifically designed electrostatic sensor is proposed in this paper to realize shaft centerline orbit reconstruction. The sensor consists of one electrostatic field excitation electrode, two sensing electrodes, and a cylindrical shield covering the three electrodes; it directly establishes the map from sensor output (voltages between sensing electrodes and shield) to shaft center position through neural network approximator.

This paper aims to explore the novel usage of electrostatic sensor for shaft centerline orbit measurement. The simulation experiment has demonstrated good performance in shaft centerline reconstruction.

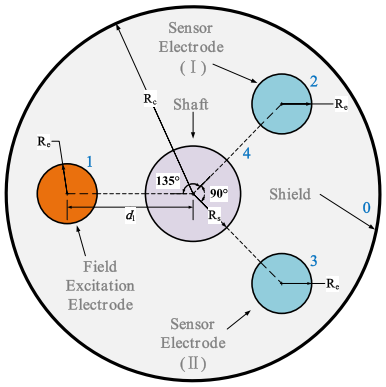

FIGURE 1. Structure of the sensor.

II. SENSING PRINCIPLE AND MEASUREMENT SYSTEM MODELING

A. SENSOR STRUCTURE

The sensor consists of a shield and three cylinder electrodes of which one is used as "field excitation electrode" while the others are used as "sensing electrodes". The three electrodes are arranged surrounding the shaft to be measured, and their spatial position is proposed in Fig. 1. The center distances between shaft and electrodes equal to d_i (i = 1, 2, 3); The radium of the shaft and the three electrodes equal to R_s (15 mm) and R_e (3 mm), respectively. The three electrodes and the shaft are shielded in a metal can shaped into a cylinder with radium R_c (48 mm) and without bottoms. The distances between the electrodes and the shaft are d_1, d_2, d_3, respectively, whose initial values are d (5 mm). Due to the length of the proposed structure is long enough, the influence of lacking bottom conductor can be ignored; The three electrodes, shaft, and the metal can constitute an electrostatic isolated system, numbered 0-4, respectively. A DC bias (24 V) is applied between conductor 0 (the shield) and conductor 1 (the field excitation electrode). The key geometry parameters are presented in Fig. 2.

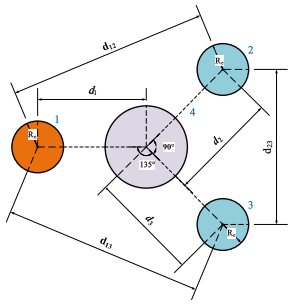

FIGURE 2. Key geometry parameters of the sensor.

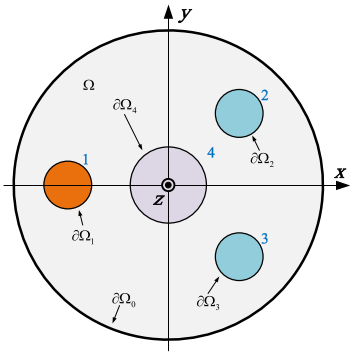

FIGURE 3. Coordinate system establishing.

B. PHYSICAL MODEL AND SENSING PRINCIPLE

1) FEM MODEL ESTABLISHING

A cylindrical coordinate system can be established whose origin is located at the bottom surface center of the shaft and the positive direction of z-axis is axially along the shaft, as is shown in Fig. 3. Ω (the air) is the solution domain with boundary $\partial\Omega_i$, $i = 0, 1, \cdots, 4$ (surfaces of shield, two electrodes, and shaft). Considering that there is no need for solving potential function inside conductor for an electrostatic problem, the solution domain does not include the electrodes and shaft entities but their surfaces.

According to electrostatic theory [10], the physical model of the measurement system can be described as following:

$$\begin{cases} \nabla^2\varphi = 0, \text{in}\Omega \\ \varphi|_{\partial\Omega_0} = 0 \\ \varphi|_{\partial\Omega_1} = U_1 \\ -\sum_i \int_{\partial\Omega_i} (\varepsilon_0 \nabla\varphi) \cdot \mathbf{n} dS = 0, \quad i = 0, 1, 2, 3, 4 \end{cases} \tag{1}$$

where U_1 is the applied field excitation potential; $\mathbf{n}$ is the outer normal vector of $\partial\Omega_i$. It is obviously that formula (1) is a typical Laplacian function with Dirichlet boundary condition.

Fig. 4 shows the geometry model built in COMSOL Multiphysics. According to aforementioned analysis, potential of excitation electrode is set to 24 V and the two sensing electrodes are set to floating potential condition; the shield is set to grounded condition as it works as zero potential reference of the electrostatic isolated system. The main physical field

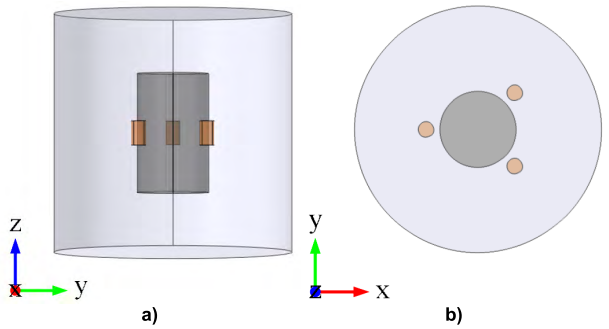

FIGURE 4. FEM model. a) Front view; b) Top view.

TABLE 1. Units for magnetic properties.

Physical Condition	Applied Geometry Object	Value
Potential	The field excitation electrode	24 V
Grounded	The shield	0 V
Floating Potential	The sensing electrodes & shaft	-

TABLE 2. Key geometry parameters of the FEM model.

Parameter	Value or Initial Value	Description
C_x	0	X-coordinate of the shaft center
C_y	0	Y-coordinate of the shaft center
d	5 mm	Initial distance between shaft and sensing electrodes
R_{shaft}	15 mm	Radium of the shaft
R_{shield}	48 mm	Radium of the shield (solution domain boundary)
$R_{electrode}$	3 mm	Radium of the three electrodes

interface setups is illustrated in Table 1, and the key geometry parameters of the FEM model is illustrated in Table 2.

It is notable that the motion of free charge on conductor surface was constrained by formula (1), which is usually used in FEM modeling but hard to obtain an analytical solution. Hence, an electrical circuit model will be put forward and used to discuss the sensor characters in the next section.

2) ELECTRIC CIRCUIT MODEL AND SENSING PRINCIPLE

According to electrostatic theory, the circuit model of the proposed measurement system can be described as a capacitance network, as is presented in Fig. 5. U_{ij} is the potential difference between the i-th and the j-th conductor, and C_{ij} is the partial capacitance between conductor i and j in the system.

The relation between charge quantity q_i of the ith conductor, C_{ij}, and U_{ij} is

$$q_i = \sum_{j \neq i} C_{ij} U_{ij} \tag{2}$$

or

$$\mathbf{q} = \mathbf{C}\mathbf{U} \tag{3}$$

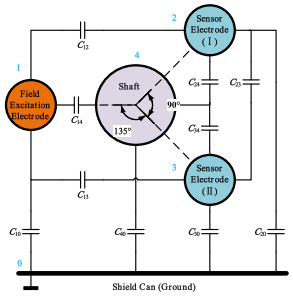

FIGURE 5. Capacitance network model of the measurement system.

where

$$\mathbf{q} = \begin{bmatrix} q_1 & q_2 & q_3 & q_4 \end{bmatrix}^{\mathrm{T}} \tag{4}$$

$$\mathbf{C} = \begin{bmatrix} C_{10} & C_{12} & C_{13} & C_{14} \\ C_{20} & C_{21} & C_{23} & C_{24} \\ C_{30} & C_{31} & C_{32} & C_{34} \\ C_{40} & C_{41} & C_{42} & C_{43} \end{bmatrix} \tag{5}$$

$$U = \begin{bmatrix} U_{10} & U_{12} & U_{13} & U_{14} \\ U_{20} & U_{21} & U_{23} & U_{24} \\ U_{30} & U_{31} & U_{32} & U_{34} \\ U_{40} & U_{41} & U_{42} & U_{44} \end{bmatrix} \tag{6}$$

Denote the equivalent capacitance of the sensor, viz., the equivalent capacitance between the shield and the field excitation electrode, as $C_{\mathrm{eq.}}$ According to Fig. 5, it is obviously that $C_{ij} = C_{ji}$, $U_{ij} = U_{ji}$. Once the shaft moves eccentrically, C_{eq} will change correspondently due to the changed relative position of conductors; then, the total charge of the conductor system will change when the new electrostatic equilibrium state is established which further affect the charge distribution of every conductor. And eventually, U_{ij} changes. Therefore, if U_{ij} is measured simultaneously during rotating, the shaft center orbit can be reconstructed. Actually, to determine one point of the shaft centerline orbit only needs 2 elements of $\mathbf{U}$: U_{20} and U_{30}, which are the only measurable quantities. This will be illustrated in the next. For convenience, denote U_{20} as U_2, and U_{30} as U_3.

It is worth mentioning that the time consumpt τ of establishing a new electrostatic equilibrium state can be ignored due to the conductors of the measurement system satisfy perfect electrical conductor condition:

$$\begin{cases} \omega \ll \tau \\ \tau \triangleq \dfrac{\varepsilon}{\sigma} \end{cases} \tag{7}$$

where ω is the shaft motion frequency; ε and σ are the permittivity and conductivity of the applied conductor material, respectively. Generally τ is of the magnitude of 10^{-17} s which is far less than the shaft motion period, so that a new electrostatic equilibrium state can be regarded as instantaneously established.

Partial capacitance matrix $\mathbf{C}$ are only concerned with the dielectric distribution, conductor geometry and the relevant position between conductors. Assume the coordinate of shaft center is $\mathbf{x} = (x, y)$. Since the conductor geometry are

invariable, and the variable spatial parameters are d_i, $\mathbf{C}$ can be presented as following equations:

$$\mathbf{C} = \mathbf{F}(\mathbf{x}) \tag{8}$$

$$\mathbf{F} = \begin{bmatrix} f_{10}(\mathbf{x}) & f_{12}(\mathbf{x}) & f_{13}(\mathbf{x}) & f_{14}(\mathbf{x}) \\ f_{20}(\mathbf{x}) & f_{21}(\mathbf{x}) & f_{23}(\mathbf{x}) & f_{24}(\mathbf{x}) \\ f_{30}(\mathbf{x}) & f_{31}(\mathbf{x}) & f_{32}(\mathbf{x}) & f_{34}(\mathbf{x}) \\ f_{40}(\mathbf{x}) & f_{41}(\mathbf{x}) & f_{42}(\mathbf{x}) & f_{43}(\mathbf{x}) \end{bmatrix} \tag{9}$$

$$\mathbf{q} = \mathbf{CU} = \mathbf{F}(\mathbf{x})\mathbf{U} \tag{10}$$

where $\mathbf{F}$ is the transfer function matrix of the electrostatic isolated system whose elements can be calculated by FEM. $\mathbf{F}$ is a bijection between $\mathbf{C}$ and $\mathbf{x}$; it is proven by means of numerical experiment and is demonstrated in the next. So far the sensing mechanism can be presented as is shown in Fig. 6.

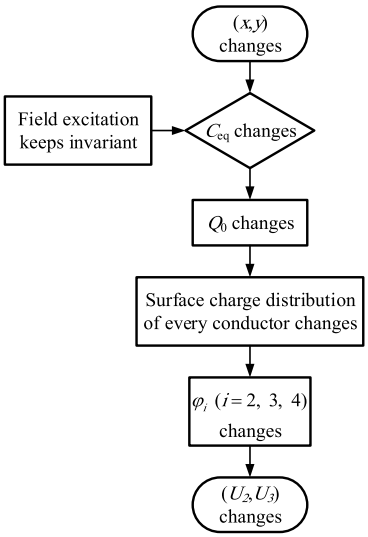

FIGURE 6. Flowchart of sensing mechanism.

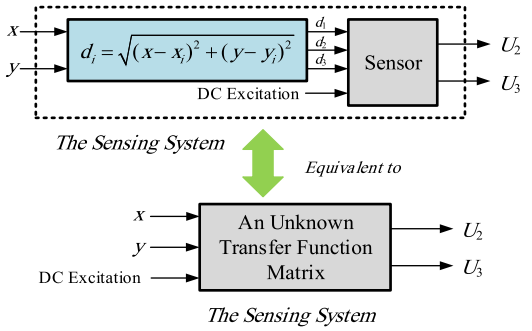

FIGURE 7. Flowchart of sensing mechanism.

According to aforementioned analysis, the sensing system can be treated as grey systems (bijection between inputs and outputs) mapping (d_1, d_2, d_3) to $\mathbf{u} = (U_2, U_3)$, or should say mapping $\mathbf{x}$ to $\mathbf{u}$. Hence, the sensing system can be abstracted to block diagram, as is shown in Fig. 7. In Fig. 7, the unknown transfer function matrix can be approach by neural network owning to the bijection relationship between $\mathbf{x}$ and $\mathbf{u}$.

III. SIMULATION ANALYSIS IGNORING MEASUREMENT CIRCUIT-INTRODUCED ERROR

Due to it is hard to generate a precisely controlled stationary centerline orbit, a simulation experiment coupling electrostatic field and object moving together that simulates the reality is carried out to validate the effectiveness of the proposed method.

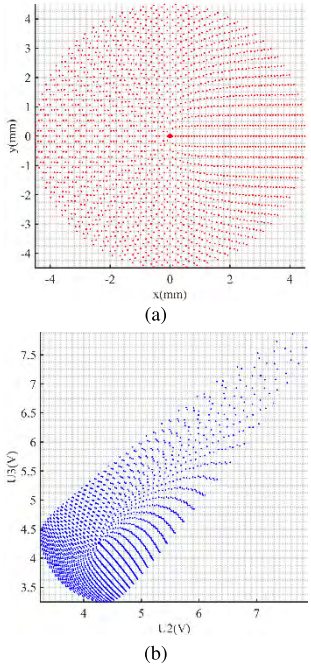

FIGURE 8. Shaft center position selection for neural network training. a) The selected shaft center positions; b) The corresponding sensor outputs.

A. SENSOR STRUCTURE

Assume the motion range of the shaft center is limited in a circular area whose boundary is 1 mm away from the electrode. Select 3101 points in such circular area, as is shown in Fig. 8-a), and the corresponding sensor output of each selected shaft center position is shown in Fig. 8-b). It is obviously that the relationship between sensor outputs and inputs is bijection. These chosen input-output pairs will be next applied to neural network training. Actually, the above conclusion can be easily proved by comparing the inputs $\mathbf{x}$ and outputs $\mathbf{u}$ using MATLAB.

B. NEURAL NETWORK FITTING AND CENTER ORBIT RECONSTRUCTION

A single-hidden layer feedforward neural network is chosen to be sensing system approximator in this paper, which includes one input layer of 2 neurons, one hidden layer of 10 neurons, and one output layer with 2 neurons. Bayesian regularization is adopted as the network training algorithm. The detailed introduction of Bayesian regularization can be found in [11], [12]. The neuron excitation function is chosen

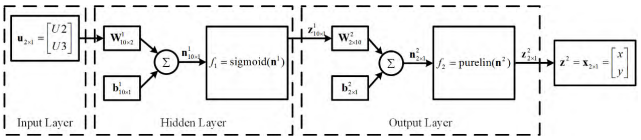

FIGURE 9. Structure of the applied neural network.

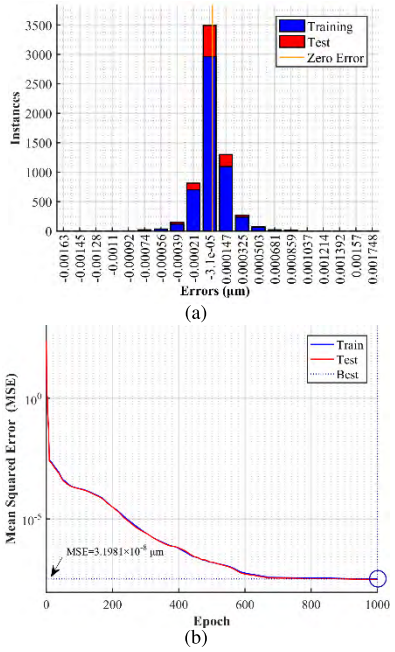

FIGURE 10. Neural network training performance. a) Error histogram of neural network training; b) Training performance vs. epoch.

to be Sigmoid function:

$$f(x) = \frac{1}{1 - e^{-x}} \tag{11}$$

The number of hidden layer neurons is determined by the following empirical formula:

$$l < \sqrt{(m+n)} + a \tag{12}$$

where l is the number of hidden layer neurons; $m = 2$, $n = 2$ represents the number of input layer neurons and output layer, respectively; $a = 8$ is an arbitrary positive constant that less than 10. The structure of the proposed neural network is shown in Fig. 9.

Take the 3101 input-output pairs chosen in section 3.1 for neural network training: 2326 instances of which are used for training, 620 for validation, and 155 for testing.

The training effect, as is shown in Fig. 10, is evaluated with absolute error and mean squared error (MSE) of neural network output and target data:

$$ERR_{\text{abs}} = |\mathbf{x}_i - \mathbf{x}_{\text{N}i}| \tag{13}$$

where $\mathbf{x}_{\text{N}i}$ represents neural network's output and $\mathbf{x}_i$ represents neural network's output;

$$MSE = \frac{1}{L}\sum_{i=1}^{L} |\mathbf{x}_i - \mathbf{x}_{\text{N}i}| \tag{14}$$

where L represents instance number of every training epoch. The best performance is obtained at epoch 1000 (MSE $= 3.1981 \times 10^{-8}\mu$m).

Five typical shaft center orbit curves that represent five kinds of mechanical fault states (donated as $\text{C}_i(x, y)$) are artificially set to COMSOL Multiphysics as parameter lists to simulating sensor's practical output curves (donated as $\text{S}_i(U_2, U_3)$). Then take every point of S_i as inputs of the trained neural network to approximate the shaft center position. The output curves of the neural network is donated as $\text{N}_i(x, y)$. The five presupposed orbit expressions are presented in Table 3.

TABLE 3. Presupposed orbits applied to test the trained neural network.

Orbit Shape	Expression	Fault Type[13]
Spiral	$\text{C}_1: \begin{cases} x = vt\cos(2\pi ft) \\ y = vt\sin(2\pi ft) \end{cases}$	Rotor friction
Circle	$\text{C}_2: \begin{cases} x = h\cos(2\pi ft) \\ y = h\sin(2\pi ft) \end{cases}$	Unbalance
Ellipse	$\text{C}_3: \begin{cases} x = a\cos(2\pi ft) \\ y = b\sin(2\pi ft) \end{cases}$	Misalignment
Ellipse (oblique)	$\text{C}_4: \begin{cases} \begin{bmatrix} x \\ y \end{bmatrix} = \begin{bmatrix} \cos\alpha & \sin\alpha \\ -\sin\alpha & \cos\alpha \end{bmatrix} \begin{bmatrix} x' \\ y' \end{bmatrix} \\ x' = a\cos(2\pi ft) \\ y' = b\sin(2\pi ft) \\ \alpha = \pi/6 \end{cases}$	Misalignment
"8" Figure	$\text{C}_5: \begin{cases} x = a\cos(2\times 2\pi ft) \\ y = b\sin(2\pi f) \end{cases}$	Misalignment (serious)

In Table 3, parameter f equals to 50 Hz, representing the rotational frequency of the shaft, and time parameter t varies from 0 to $1/f$ with step length of which is 4×10^{-4} s; $v = 3$ mm/s represents radial velocity of the shaft; $h = 30$ μm represents the maximum radial displacement of the shaft; $a = 10$ μm and $b = 25$ μm represent the major and short semi-axis parameters of the presupposed ellipse orbits, respectively. The curves of each presupposed orbit and the corresponding sensor outputs are shown in Fig. 11.

In Fig. 11, the absolute error can be calculated by formula (15):

$$err_i = \sqrt{D(\mathbf{x}_i, \mathbf{x}_{\text{N}i})} \times 100\% \tag{15}$$

where $D(\mathbf{x}_i, \mathbf{x}_{\text{N}i})$ represents the distance between the i-th points of C_i and N_i:

$$D(\mathbf{x}_i, \mathbf{x}_{\text{N}i}) \triangleq (x_i - x_{\text{N}i})^2 + (y_i - y_{\text{N}i})^2 \tag{16}$$

The root mean square error (RMSE) and the maximum quoting error (MQE) of the neural network fitting is shown in Table 4. They are calculated by formula (17) and (18):

$$RMSE = \sqrt{\frac{1}{n}\sum_{i=1}^{n} D(\mathbf{x}_i, \mathbf{x}_{\text{N}i})} \tag{17}$$

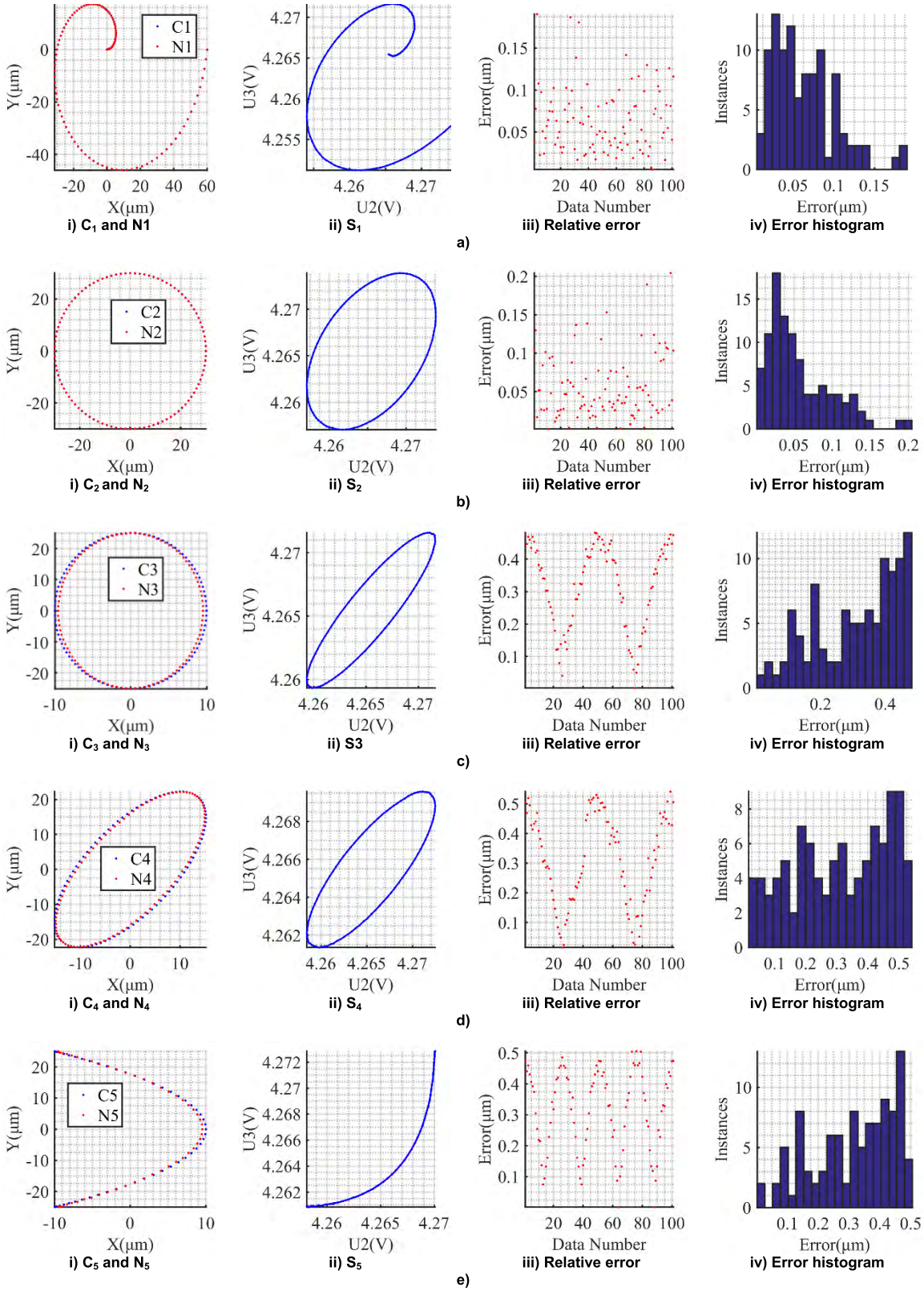

FIGURE 11. Shaft centerline orbit reconstruction performance. a) Adopt C_1 as the presupposed orbit; b) Adopt C_2 as the presupposed orbit; c) Adopt C_3 as the presupposed orbit; d) Adopt C_4 as the presupposed orbit; e) Adopt C_5 as the presupposed orbit.

TABLE 4. Total RMSE and MQE of the 5 tests.

Test Number	1	2	3	4	5
RMSE (μm)	0.074319	0.069622	0.338786	0.345685	0.341414
MQE (%)	0.422711	0.453819	1.069618	1.202206	1.122083

where n is the number of data points of (x_i, y_i) and (x_{Ni}, y_{Ni}).

$$MQE = \frac{\max\{err_i\}}{FS} \times 100\% \tag{18}$$

where FS presents the full scale of the sensor. Here, FS is set to 45 μm.

Fig. 11 and Table 4 have demonstrated the good performance of the proposed neural network. It is noticeable that the spatial position selection for neural network training is sparse compared with the presupposed orbits applied to reconstruction experiment; but the trained neural network shows good performance in mapping sensor output (U_2, U_3) to shaft center position (x,y), which has proved the conclusion put forward in *Section II-2)* that $\mathbf{F}$ is a bijection between $\mathbf{C}$ and $\mathbf{x}$ once again.

So far, the simulation experiments have proved the effectiveness of the proposed theoretically. It can be read from Table 4 that the RMSE of the proposed method is within 0.4μm in ideal situation, which is potential qualified to shaft centerline reconstruction.

IV. CONCLUSION

The main purpose of this paper is to provide researchers with a new idea and an non-contact way to easily and quickly obtain shaft centerline orbit. This paper aims at the theoretical analysis of the proposed sensor as well as its corresponding measurement method.

According to the above analysis, the proposed sensing principle has been proven to be correct and qualified to shaft center orbit monitoring. The proposed sensor is actually a kind of ''coordinate sensor'' rather than a displacement sensor, because the sensor's input is shaft center position $\mathbf{x}$. The relationship between $\mathbf{x}$ and sensor output $(\mathbf{u})$ is directly established by a neural network approximator.

In the further study, we are to aim at the following aspects:

1) According to electrostatic field theory, some parameters of the sensor (mainly include electrode length, electrode width, and the field excitation voltage) that influence the sensor performance (such as frequency response and sensor resolution) should be optimized; it is better if the analytical expression between sensor parameter and sensor performance should be derived which has significant meaning to sensor design.

2) The corresponding neural network structure and parameters need to be further optimized to obtain a more accurate approximation.

3) To measure the potential difference between reference ground and floating conductor, which differs from traditional voltage measurement, is a challenging work. It is because once measurement circuit or instrument is introduced, the established electrostatic equilibrium will be broken and the sensing system's structure is changed, too. Thus an electromagnetic transient behaviour will happen to the measurement system that cannot be described only by electrostatic equations; the sensing system will turn to an electrodynamic object. Therefore, the physical realization of floating measurement circuit needs to be further studied, which requires very high input impedance and ultra-low leakage current. Meantime, the realization details, for example, weather use the sensor shield (the ground point of the applied field excitation DC source) as the ground point of measurement circuit or not and how to overcome the noise introduced by an extreme large resistance, need to be studied.

REFERENCES

[1] F. Xiang-Qian, L. Guang-Lin, J. Jing, and L. You-Ping, ''Automatic identification of axis orbit based on both wavelet moment invariants and neural network,'' *Wuhan Univ. J. Nat. Sci.*, vol. 8, no. 2, pp. 414–418, Jun. 2003.

[2] Z. Feng, X. Song, D. Xue, Y. Xie, and D. Deng, ''Survey of vibration fault diagnosis of rotational machinery,'' *J. Vib. Shock*, vol. 20, no. 4, pp. 34–39, Dec. 2001.

[3] M. R. Nabavi and S. N. Nihtianov, ''Design strategies for eddy-current displacement sensor systems: Review and recommendations,'' *IEEE Sensors J.*, vol. 12, no. 12, pp. 3346–3355, Dec. 2012.

[4] T. Yamaguchi and M. Ueda, ''An active sensor for monitoring bearing wear by means of an eddy current displacement sensor,'' *Meas. Sci. Technol.*, vol. 18, no. 1, pp. 311–317, Dec. 2006.

[5] J. B. Gajewski, ''Electrostatic nonintrusive method for measuring the electric charge, mass flow rate, and velocity of particulates in the two-phase gas–solid pipe flows—Its only or as many as 50 years of historical evolution,'' *IEEE Trans. Ind. Appl.*, vol. 44, no. 5, pp. 1418–1430, Sep./Oct. 2008.

[6] J. Shao, J. Krabicka, and Y. Yan, ''Velocity measurement of pneumatically conveyed particles using intrusive electrostatic sensors,'' *IEEE Trans. Instrum. Meas.*, vol. 59, no. 5, pp. 1477–1484, May 2010.

[7] L. Wang, Y. Yan, Y. Hu, and X. Qian, ''Rotational speed measurement through electrostatic sensing and correlation signal processing,'' *IEEE Trans. Instrum. Meas.*, vol. 63, no. 5, pp. 1190–1199, May 2014.

[8] L. Li, X. Wang, H. Hu, and X. Liu, ''Use of double correlation techniques for the improvement of rotation speed measurement based on electrostatic sensors,'' *Meas. Sci. Technol.*, vol. 27, no. 2, Dec. 2015, Art. no. 025004.

[9] Y. Hu, Y. Yan, L. Wang, X. Qian, and X. Wang, ''Simultaneous measurement of belt speed and vibration through electrostatic sensing and data fusion,'' *IEEE Trans. Instrum. Meas.*, vol. 65, no. 5, pp. 1130–1138, May 2016.

[10] B. D. Popovic, ''Electromagnetic field theorems,'' *IEE Proc. A-Phys. Sci., Meas. Instrum., Manage. Educ.-Rev.*, vol. 128, no. 1, pp. 47–63, Mar. 1981.

[11] F. D. Foresee and M. T. Hagan, ''Gauss-Newton approximation to Bayesian learning,'' in *Proc. Int. Conf. Neural Netw.*, vol. 3, Houston, TX, USA, Jun. 1997, pp. 1930–1935.

[12] D. J. C. MacKay, ''Bayesian interpolation,'' *Neural Comput.*, vol. 4, no. 3, pp. 415–447, 1992.

[13] P. Guo, X. Luo, Y. Wang, L. Bai, and H. Li, ''Identification of shaft centerline orbit for hydropower units based on particle swarm optimization and improved bp neural network,'' *Proc. CSEE*, vol. 31, no. 8, pp. 93–97, Mar. 2011.

KAIHAO TANG received the B.Eng. degree from Chang'an University, Xi'an, China, in 2015. He is currently pursuing the Ph.D. degree in instrument science and technology with the School of Electrical Engineering, Xi'an Jiaotong University, Xi'an.

His current research interests include theory and application of electrical tomography, multiphase flow measurement and instrumentation, electromagnetical sensing, and digital image and signal processing.

HONGLI HU (M'14) received the M.Sc. and Ph.D. degrees in electrical engineering and power engineering from Xi'an Jiaotong University, Xi'an, China, in 1991 and 2005, respectively.

Since 1991, he has been engaged in teaching and research of measurement and control engineering at the School of Electrical Engineering, Xi'an Jiaotong University, where he is currently with the Institute for Thermal Engineering. He is also a Professor and a Leader of the Smart Transducer Research Group. He has authored more than 50 research papers. His current research interests include the measurement of multiphase flow, process tomography, and smart transducer systems.

Dr. Hu is also a member of the Editorial Advisory Board of Flow Measurement and Instrumentation.

LIN LI received the B.Eng. degree in measurement-control technology and instrumentation from Xi'an Jiaotong University, Xi'an, China, in 2013, where he is currently pursuing the Ph.D. degree with the Department of High Voltage and Electrical Insulation Technology.

His current research interests include electrostatic sensing and signal processing.

YONG QIN received the B.Sc. and M.Sc. degrees in transportation automation and control engineering from Shanghai Railway University, China, in 1993 and 1996, respectively, and the Ph.D. degree in information engineering and control from the China Academy of Railway Sciences, in 1999.

He is currently a Professor and the Vice Dean with the State Key Laboratory of Rail Traffic Control and Safety, Beijing Jiaotong University. He has authored or coauthored more than 100 publication papers (SCI/EI), one ESI highly cited paper, and five books. He holds 23 patents granted, including two USA patents. His research interests include prognostics and health management for railway transportation systems, transportation network safety and reliability, rail operation planning and optimization. He is also the member of the IEEE ITS and the IEEE RS and a Senior Member of the IET. He received 11 science and technology progress awards of the ministry.

XIAOXIN WANG received the Ph.D. degree in instrument science and technology from Xi'an Jiaotong University, Xi'an, China, in 2017.

She is currently engaged in teaching and research of measurement and control engineering at the School of Electronic Engineering, Xi'an Shiyou University. Her current research interests include multiphase flow measurement, capacitance sensor, electrostatic sensor, electrical capacitance tomography (ECT), and data fusion.